Transfer Learning from Simulations on a Reference Anatomy for ECGI in Personalised Cardiac Resynchronization Therapy

Sophie Giffard-Roisin, Hervé Delingette, Thomas Jackson, Jessica Webb, Lauren Fovargue, Jack Lee, Christopher A Rinaldi, Reza Razavi, Nicholas Ayache, Maxime Sermesant

Transfer Learning from Simulations on a Reference Anatomy for ECGI in Personalised Cardiac Resynchronization Therapy

Sophie Giffard-Roisin*, Hervé Delingette, Thomas Jackson, Jessica Webb, Lauren Fovargue, Jack Lee, Christopher A. Rinaldi, Reza Razavi, Nicholas Ayache, Maxime Sermesant*

***Abstract*—*Goal:* Non-invasive cardiac electrophysiology (EP) model personalisation has raised interest for instance in the scope of predicting EP cardiac resynchronization therapy (CRT) response. However, the restricted clinical applicability of current methods is due in particular to the limitation to simple situations and the important computational cost. *Methods:* We propose in this manuscript an approach to tackle these two issues. First, we analyse more complex propagation patterns (multiple onsets and scar tissue) using relevance vector regression and shape dimensionality reduction on a large simulated database. Second, this learning is performed offline on a reference anatomy and transferred onto patient-specific anatomies in order to achieve fast personalised predictions online. *Results:* We evaluated our method on a dataset composed of 20 dyssynchrony patients with a total of 120 different cardiac cycles. The comparison with a commercially available electrocardiographic imaging (ECGI) method shows a good identification of the cardiac activation pattern. From the cardiac parameters estimated in sinus rhythm, we predicted 5 different paced patterns for each patient. The comparison with the body surface potential mappings (BSPM) measured during pacing and the ECGI method indicates a good predictive power. *Conclusion:* We showed that learning offline from a large simulated database on a reference anatomy was able to capture the main cardiac EP characteristics from non-invasive measurements for fast patient-specific predictions. *Significance:* The fast CRT pacing predictions are a step forward to a non-invasive CRT patient selection and therapy optimisation, to help clinicians in these difficult tasks.**

***Index Terms*—Cardiac Electrophysiology, ECG Imaging, Inverse Problem of ECG, Personalisation.**

I. Introduction

HEART failure is a major health issue in Europe affecting 6 million patients and growing substantially because of the ageing population and improving survival following myocardial infarction. The poor short to medium term prognosis of these patients means that treatments such as cardiac resynchronisation therapy (CRT) can have substantial impact [1], [2]. However, these therapies are ineffective in 30% of the treated patients and involve significant morbidity and substantial cost. To this end, the precise understanding of the patient-specific cardiac function can help predict the response to therapy and therefore select the potential candidates and optimise the therapy.

S. Giffard-Roisin (sophiegif.github.io), H. Delingette, N. Ayache and M. Sermesant (maxime.sermesant@inria.fr) are with Asclepios Research Group, Université Côte d'Azur, Inria, France.

T. Jackson, L. Fovargue, J. Lee, J. Webb, C. Rinaldi and R. Razavi are with Division of Imaging Sciences and Biomedical Engineering, King's College London, London, UK.

Estimating accurately electrophysiological (EP) patient-specific model parameters is then crucial, and it often involves invasive measurements [3]. In order to replace these invasive measurements -at risk for the patient-, some studies proposed to personalise the cardiac EP model from body surface potential mappings (BSPM) [4]–[6]. In one of them [5], the onset activation location and the global conduction velocity were estimated in different pacing locations for several patients using a patient-specific simulated training set. However, personalisation may often be needed in more complex situations, such as multiple activation onsets or heterogeneous myocardial tissue (scar). Besides, such patient-specific methods are time consuming because a large number of model simulations are needed: the total computational time of one model personalisation [5] was more than 5 hours on our cluster using parallel computing.

The aim of this article is to develop a reference anatomy model allowing us to perform a common and offline learning. While reducing considerably the computational time of online inference, it also allows to multiply the pathological configurations in the simulated training set as it is built only once. We have thus extended the cardiac EP model personalisation to infarct situations and applied it to a 20 patient database where the BSPM were recorded using the CardioInsight[1] jacket now commercially available. The personalised model was then used to predict the activation under different pacing configurations typically used for CRT.

A. EP Model-based Inverse Problem of Electrocardiography

BSPM data has been widely used in the last decades to directly compute the cardiac action potentials by solving an ill-posed inverse problem: finding the transfer matrix linking the torso potentials to the cardiac sources in terms of action potentials or impressed currents [7]. For example, the 3DCEI approach minimizes the use of physiological constraints and was thus applied to various clinical conditions [8]–[11]. Some electrocardiographic imaging (ECGI) methods are integrating physiological and model-based priors in a Bayesian framework [12], [13]. The work by Li and He [4] solves the inverse problem by means of heart-model parameters (onset activation location) and was validated with in vivo studies [14]. It was further developed for localizing PVC origins from convolutional neural networks [15]. With a known onset activation

[1]ECVUE, CardioInsight Technologies Inc., Cleveland, Ohio

location, the estimation of heterogeneous myocardial conduction using a Bayesian framework has been recently studied by Dhamala et al. [6]. The use of non-invasive personalised cardiac parameters for the prediction of new situations (such as pacing procedures) has been tackled on a few cases only and with a global conduction velocity parameter [5].

B. Reference Anatomy in ECGI

These personalisations of EP cardiac model parameters from BSPM data rely on time-consuming patient-specific computations. Because of the natural similarity of the anatomical structures between patients, a reference anatomy can be used.

One study showed the importance of the interindividual variability (averaged standard deviation) of electrocardiograms (ECG) on 25 healthy subjects [16]. A large part of this variability is due to the heart position and orientation relative to electrodes. In terms of geometry, the larger variations are found for the heart long axis angle. Swenson et al. [17] also revealed the importance of cardiac angulation in the ECG forward problem. Another study showed that ECG imaging is sensitive to global anatomical parameters such as the heart orientation and location with regard to the lead positions [18]. The use of a reference anatomy model, able to represent every patient, is thus a difficult task. Hoekema et al. [16] showed that by only moving the electrodes in a frontal plane to a common reference, the interindividual variability is not reduced because the heart orientation is not preserved. Another study created a patient-specific adapted torso model by stretching and squeezing a standard torso model according to the measures [19]. They concluded that it was crucial to adapt both the outer shape of the torso model and the position of electrodes according to reality. Yet, it has been also shown that some adapted ventricle-torso standard model were able to get good ECGI results while excluding local geometrical details [20], [21]. Lastly, a recent study uses a generic ventricle-torso model in order to build an EP model training set [15], however the training phase had to be patient-specific as the generic geometry was first registered to every patient geometry. To the best of our knowledge, the goals of these geometrical models were only to simplify the anatomical modelling process. However, a study has recently tackled the interindividual variability by separating the factors of variation throughout a deep network using a denoising autoencoder on a large ECG dataset [22] for learning the ventricular tachycardia origin. Inter-subject variations coming from cardiac EP differences and geometry differences are however not separable, so a personalised EP model could not be estimated with this approach.

C. Contributions

The different contributions of this manuscript are:

- A novel reference anatomy approach able to easily represent every patient with preserved heart orientation and position with respect to the lead positions. It reduces considerably the computational cost of the personalisation.
- A simulated common database composed of 5 000 heart-torso EP simulations having random parameter values in terms of onsets, global conduction velocity value and scar localisation.
- An EP model-based ECGI technique able to personalise an EP cardiac model from a sinus rhythm BSPM sequence. It is based on a dimensionality reduction of the myocardial shape and a sparse relevance vector regression.
- An evaluation on an important database of clinical data composed of 20 patients with a CRT device, and with a comparison to a commercially available ECGI method.
- The simulated predictions of 100 different QRS under pacing compared with the measured BSPM (unseen data) and the commercially available ECGI mapping.

D. Outline of the Manuscript

In the following section II we will present our prediction framework (Figure 1): the clinical data, our reference anatomy model, the simulated EP database and the personalisation of the sinus rhythm sequence. Section III is dedicated to the results and the pacing predictions. Finally, section IV discusses the different aspects of the method.

II. Materials and Methods

A. Clinical Data

Our 20 patients dataset is composed of BSPM signals, ventricular myocardial geometry, torso leads and pacing leads locations. All patients have dyssynchrony (either left or right bundle branch block) and were implanted with a biventricular pacemaker (see Table I). The BSPM potentials (from a CardioInsight jacket) were acquired at a sampling rate of 1kHz during one QRS complex by 200 to 250 torso sensors. The protocol of this study was approved by the local research ethics committee. The approximated myocardial surface, the location of the torso sensors and the pacing leads were extracted from the 3D CT scanner image. In the stimulation optimisation procedure, cardiologists performed several recordings corresponding to different pacing combinations and delays between a right ventricular (RV) endocardial and a left ventricular (LV) epicardial pacing leads. For almost all patients, a *LV pacing* alone and a *RV pacing* alone were performed, together with the 3 following biventricular pacings: *simultaneous*, *LV 40ms* (LV lead ahead by 40ms) and *RV 40ms* (RV lead ahead by 40ms). An atrial pacing was active 200ms to 100ms before the ventricular pacings. A *sinus rhythm* sequence was also recorded on patients that do not have complete heart blocks. In total, 120 different settings were studied.

B. BSPM Reference Anatomy

1) Transformation to the Reference Anatomy: In this work, every patient p has a geometry data composed of the 3D biventricular cardiac geometry noted c_p and $s_p = \{s_p^j\}_{j=1:N}$ the locations of the N torso sensors. We define a cardiac and BSPM reference anatomy template $\{c_T; s_T\}$ with $s_T = \{s_T^i\}_{i=1:M}$ onto which every patient data will be transformed.

The current dipole approach formulated in the volume conductor theory [23] has proven its efficiency in BSPM

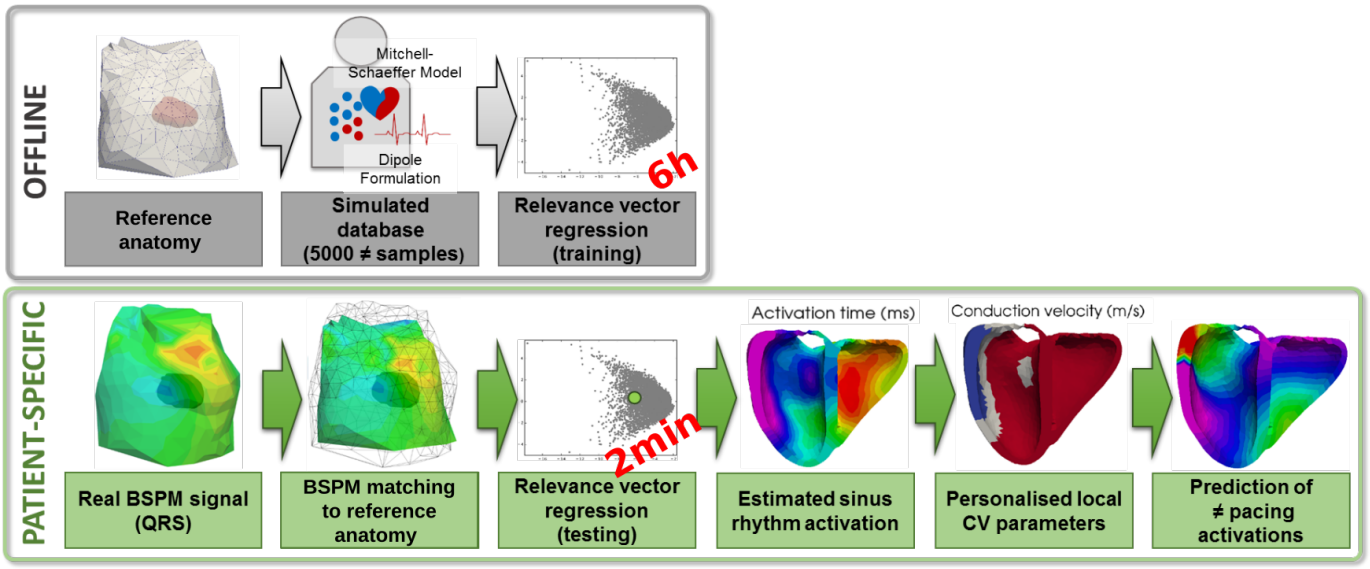

Fig. 1. Fast model-based prediction pipeline: the database composed of 5000 EP simulations and the activation map regression training are common for the 20 patients.

TABLE I
CRT PATIENTS. BASELINE INFORMATION OF THE 20 PATIENTS TREATED.

Id	Age	Gen.	Block type	Etiology	SR
1	67	M	LBBB	ICM	X
2	72	M	LBBB	HCM	
2 6M*	72	M	LBBB	HCM	X
3	82	M	LBBB	*NA*	X
4	49	F	LBBB	NICM	X
5	79	M	RBBB	ICM	X
6	87	M	LBBB	NICM	
7	62	M	LBBB	ICM	X
8	87	M	LBBB	ICM	X
9	77	M	LBBB	*NA*	X
10	69	F	LBBB	NICM	
11	49	M	LBBB	NICM	X
12	62	F	LBBB	*NA*	X
13	59	M	LBBB	ICM	X
14	82	F	LBBB	*NA*	
15	76	M	RBBB	NICM	X
16	55	M	LBBB	*NA*	X
18	49	M	LBBB	*NA*	X
19	78	M	LBBB	*NA*	X
20	73	M	LBBB	*NA*	X
22	71	M	LBBB	*NA*	X

*NA = information not available; SR = sinus rhythm sequence available; LBBB/RBBB = Left/Right bundle branch block; ICM/NICM/HCM = ischemic/non-ischemic/hypertrophic cardiomyopathy; *: patient #2 was acquired 2 times with a 6-months follow-up.*

calculation [5]. The electric potential $\Psi^v(s_p^j)$ generated by the volume element v and measured at the torso electrode s_p^j is driven by the scalar product (j_{eq}^v, vs_p^j) between the equivalent current density j_{eq}^v of every cardiac volume element v and the vector directed from v to the torso electrode s_p^j (further divided by the cubic norm of the distance). Consequently, the shape of the jth BSPM signal $\Psi^v(s_p^j)$ is closely linked to the direction of vs_p^j. This result is echoing the conclusions of the ECGI sensitivity studies (see section I-B) showing how the ECG signal is sensitive to the heart orientation and location with respect to the lead positions [18].

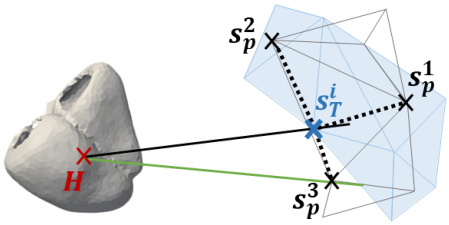

(a) Schematic simple minimal distance matching

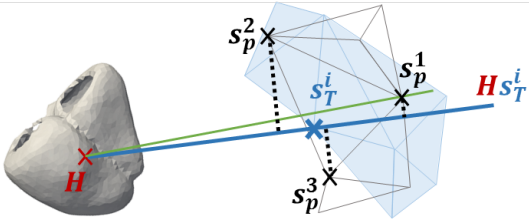

(b) Proposed matching by best preserving the directional potential

Fig. 2. Reference anatomy: matching between one template torso electrode s_T^i and the patient electrodes s_P. (a) By using a minimal distance between electrodes, the matched electrode would be s_P^3. (b) With the proposed method, the minimal distance to the ray Hs_T^i indicates a matching to the electrode s_P^1. The directional potential is thus best preserved.

First, we propose to rigidly register the cardiac geometry c_p to the template c_T (it is done interactively, as c_p is only a coarse epicardial surface and c_T a complete biventricular tetrahedral mesh), and we apply the same transformation to the electrodes s_P. We define H as the center of mass of the template cardiac geometry, and Hs_T^i as the ray from H towards the template torso sensor s_T^i. We propose the following matching between the template electrodes and the

electrodes of a new patient p:

$$\forall i \leq M,\ \Psi(s_T^i) = \Psi(s_p^j)$$
$$\text{with } j = \arg\min_k \left(dist\left(s_p^k, Hs_T^i\right)\right)$$

This matching between electrodes is not bijective. Nevertheless, the advantages of this approach are that measured BSPM signals are not modified and the directional potential is best approximated by identifying the sensor that is the closest to the direction wanted (see Figure 2). This projection, allowing the use of a reference simulated database, can also be seen as a transfer learning method between the reference domain and the patient-specific domain. The final distance $dist(s_p^k,\ Hs_T^i)$ of the matched electrode to the ray can be a measure of uncertainty: the larger the distance, the larger the uncertainty that may be introduced. The mean distance among the 20 patients was less than 2 cm.

2) Choice of the template: The choice of the template reference anatomy $\{c_T; s_T\}$ is important as c_T has to represent the general shape of the myocardium, and the torso sensors s_T should be located in relevant positions so that every patient would not be too far from it. In this study, we used a healthy cardiac mesh of 4K vertices and the 251 torso sensors s_T from one of our patients having standard torso width and rotation (patient #22, selected manually). One could estimate a mean shape, but for simplicity and consistency reasons we used real geometries. In Figure 3 is shown an example of the matching between an original BSPM signal and its translation to the torso geometry.

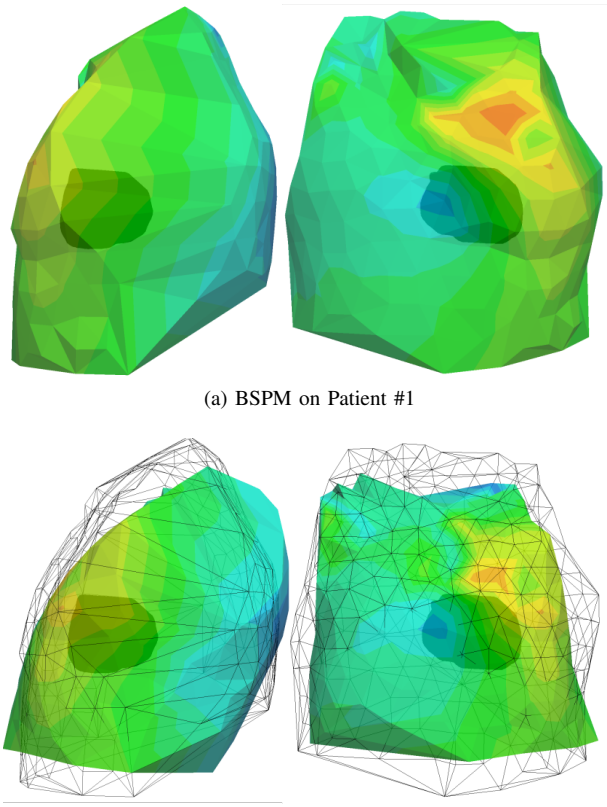

(a) BSPM on Patient #1

(b) Projection of the BSPM on the template torso

Fig. 3. Example of measured BSPM signal matching between the torso of patient #1 and the template, the color represents the voltage at one time point from blue (minimal) to red (maximal). (a) original BSPM signal on the torso of patient #1. (b) projected signal using the proposed matching method on the template, in wireframe are the original torso contours.

C. Offline Simulated Common Database

1) Simulated Database: As we do not have ground-truth intra-cardiac measurements on the 20 patients, it is difficult to learn inter-patient information in order to personalise the EP cardiac model. In order to generate a common large database with detailed cardiac data, we used EP simulations on the reference anatomy to generate 5 000 virtual cases with different parameter values. One simulation runs in approximately 2 minutes on our cluster (CPU core Xeon 2.6GHz). This offline database was used as the training set for all the personalisations of the cardiac EP model, reducing its online computational cost.

2) Forward Electrophysiological Model: On the reference myocardial mesh, the cardiac fiber orientations were estimated with a rule-based method (elevation angle between $-70°$ to $70°$). We simulated the anisotropic electrical activation of the heart using the monodomain version of the Mitchell-Schaeffer EP model [24]. One of the main parameter of the model is the local myocardial conduction velocity c (linked to the diffusion d by $cf \propto \sqrt{d}$. Our forward method is based on a simplified framework composed of sources and sensors in an infinite and homogeneous domain. We modelled every myocardium volume element (tetrahedron) as a spatially fixed but time varying current dipole. We computed simultaneously the cardiac electrical sources and body surface potentials. As shown a related study [5], the modelled BSPM signals are similar to the result of a standard boundary elements method, so the unbounded conductor is a valid approximation in this case.

3) Variety of Simulations and Parameter Ranges: In order to simulate a large variability of activation maps and their related BSPM signals, 3 groups of cardiac EP parameters were randomly modified. First, the activation onset location was randomly selected among the endo- and epi- surface vertices of the cardiac mesh. In order to simulate some more complex and realistic situations, an additional second onset location was selected for every simulation [25]. Secondly, the global myocardial conduction velocity c was randomly picked in a clinically acceptable range $[0.3, 0.7] m/s$. Third, in order to capture the conductivity heterogeneity we modelled scar tissue as having no reaction term in the Mitchell-Schaeffer model and a diffusivity reduction of 80%. A varying scar location on the LV with a random and realistic shape [26] was added in 50% of the simulations.

D. Relevance Vector Regression for Sinus Rhythm Personalisation

1) Sinus Rhythm Activation Map Estimation: Using the reference simulated database, we wanted to personalise each patient's EP behaviour from the cardiac at-rest recordings, i.e. the *sinus rhythm* sequence. For the patients where the *sinus rhythm* was not available because of complete heart blocks

(see Table I), we used the *RV pacing* sequence. The different parameters (activation onset locations, conductivity, presence of scar tissue) are linked together and their contributions in the resulting BSPM signals are hardly separable. We therefore estimated them at the same time. Because of the large variety of parameters, we chose to regress the whole cardiac activation map (the myocardial depolarisation times) from the BSPM signals. We first described the BSPM signals as a feature vector and we used a dimensionality reduction of the representation of the spatial domain given by the myocardial shape. A relevance vector regression was performed between the BSPM features and the reduced activation maps. The first part of the regression (the training, taking 6 hours to compute on average on our cluster) is common to every patient and was performed offline, while only the second step is patient-specific (the testing, taking 2 minutes to compute on average).

2) BSPM Feature Description: For every patient, the torso sensors were matched with the transformation described in Section II-B1 to the 251 leads of the template torso. Because the reference electrode was not localized, the mean BSPM signal was first subtracted to each signal. Then each signal was normalized and smoothed with a local Gaussian filter. We defined specific features from the QRS sequence of every torso leads. Specifically, 7 features were extracted from each of the 251 QRS signals (figure 4). One BSPM sequence was then represented as the feature vector x_i of size L=7x251.

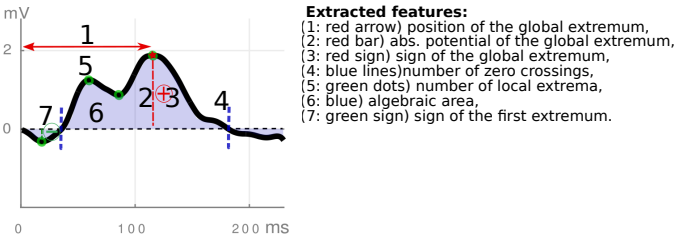

Fig. 4. Example of BSPM for one torso sensor with the extracted features.

3) Dimensionality Reduction of the Myocardial Shape: The myocardial tetrahedral mesh can have a large number of elements or vertices. At the same time, the signal to be reconstructed, the activation map, is strongly correlated spatially due to the propagation of the electric potential throughout the myocardium. Therefore, it is meaningful to reduce the dimension of the regression variable, the activation times. A simple way would be to use a coarser mesh but this would be at the expense of reducing the accuracy of the onset locations. Instead, we proposed to use a hierarchical decomposition of the mesh, naturally provided by the eigenmodes of a structural matrix. To this end we chose the eigen-decomposition of the stiffness matrix associated with the Laplacian operator of the tetrahedral shape.

This decomposition has been widely used in various spectral shape analysis [27], [28] and is closely related to the modes of vibration of the myocardium. The extracted eigenvectors are naturally sorted by ascending order of spatial frequency. By selecting the first eigenmodes, we only kept the modes with the lowest frequencies corresponding to the largest spatial variations. If we call $\mathbf{t}$ the vector of N activation times at each vertex of the myocardial mesh, we get the following reduction and reconstruction formulas:

$$\mathbf{t}_{red} = \mathbf{V}_M \mathbf{t} \ ; \ \mathbf{t}_{rec} = {\mathbf{V}_M}^T \mathbf{t}_{red}$$

with $\mathbf{t}_{red}$ the coordinates of $\mathbf{t}$ in the reduced space, $\mathbf{V}_M$ the $N \times M$ matrix of the first M eigenvectors of the stiffness matrix, and $\mathbf{t}_{rec}$ the reconstructed activation times. The matrix V_M is independent of $\mathbf{t}$ and is thus computed only once. An example of reconstructed activation map (on 4K vertices) using $M = 400$ modes is shown in Figure 5c. From Figure 5a, we can see that the mean reconstruction error was less than 1.5 ms (max: 8 ms) for 400 modes.

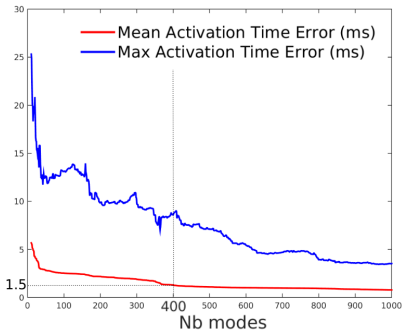

(a) Reconstruction error

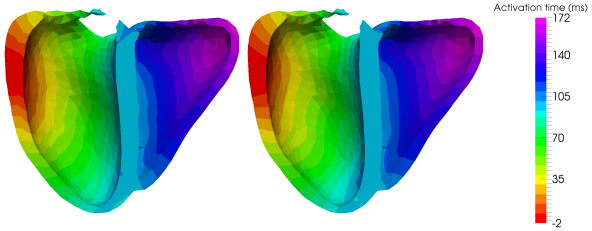

(b) Original (c) Reconstruction

Fig. 5. Example of reconstruction of an activation map (on 4312 vertices) from the eigenvectors of the stiffness matrix: (a) Reconstruction error wrt. the number of modes (b) original activation map (c) reconstructed activation map from 400 modes.

4) Relevance Vector Regression: In order to regress the myocardial activation times from the BSPM features, we used the relevance vector regression (RVR) method [29]. This approach will perform a non-linear combination of the training set in order to give a personalised EP estimation. The sparse kernel regression is based on a sparsity inducing prior on the weight parameters within a Bayesian framework. Unlike the commonly used Elastic-Net or Lasso approaches (based on L1 Norm a.k.a Laplacian prior), the RVR method does not require to set any regularization parameters through cross-validation. Instead, it automatically estimates the noise level in the input data and performs a trade-off between the number of basis (complexity of the representation) and the ability to represent the signal. Furthermore, unlike SVM regression or Elastic-Net, it provides a posterior probability of the estimated quantity which is reasonably meaningful if that quantity lies inside the training set cloud of solutions.

The RVR estimates the weights $\mathbf{w}$ so that we can predict $\mathbf{y} \in R^M$ (here an activation map in the reduced space) from

an input $\mathbf{x} \in R^L$ (here a BSPM feature vector) with a non-linear relationship between $\mathbf{x}$ and $\mathbf{y}$ as $\mathbf{y} = \mathbf{w}^T\Phi(\mathbf{x})$ where Φ is the non-linear mapping. We consider our dataset of input-target pairs $\{\mathbf{x}_i, \mathbf{t}_i\}_{i=1}^K$ where we assume that each target $\mathbf{t}_i$ represents the true model $\mathbf{y}_i$ with an addition of a Gaussian noise $\epsilon_i = \mathcal{N}(0, \sigma^2)$:

$$\mathbf{t}_i = \mathbf{w}^T\Phi(\mathbf{x}_i) + \epsilon_i \quad (1)$$

The complexity of the learned relationship between $\mathbf{x}$ and y is constrained by limiting the growth of the weights $\mathbf{w}$. This is done by imposing a zero-mean Gaussian prior on w_i:

$$P(w_i) = \mathcal{N}(0, \alpha_i^{-1}) \quad (2)$$

where the α_i are hyperparameters modifying the strength of each weight's prior. $\alpha = \{\alpha_i\}_{i=1}^K$ and σ are estimated from a marginal likelihood maximisation [30] via an efficient sequential addition and deletion of candidate basis functions (or relevant vectors). Because the optimal values of many α_i are infinite, the RVR only selects the BSPM input set that can best explain the activation map in the training set, thus limiting the risk of overfitting.

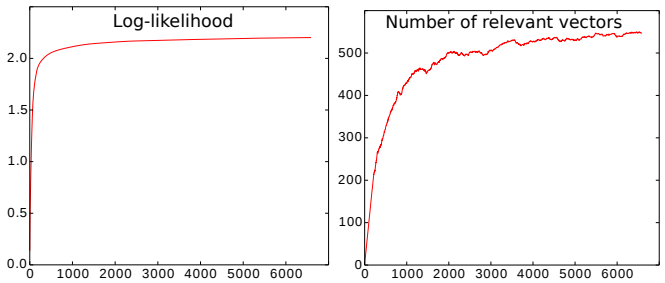

(a) Log-likelihood evolution (b) Nb of relevant vectors evolution

Fig. 6. Iterations of the relevance vector regression training on the first mode.

RVR is a multivariate but single-valued approach and therefore the regression was directly performed on the reduced space of section II-D3: only 400 regressions are needed to perform an estimation of more than 4K activation times. In our setting, a training input-target pair corresponds to a BSPM feature vector $\mathbf{x}_i$ and its related activation map projected on one mode of the reduced space $t_{red,i}^m$. We used Gaussian kernels for the non-linear mapping Φ with a kernel bandwidth of 1e4. The algorithm[2] evolution on the first shape mode (Figure 6) shows a rapid convergence even if small changes in the number of relevant vectors are still visible after 3000 iterations. The mean number of retained relevant vectors during the training phase was 178 (over 5000 training vectors). The testing phase was then performed independently on every patient: from the measured BSPM feature vector $\mathbf{x}$ we regressed the activation map estimation $\mathbf{t}$.

5) Local Conduction Velocity Parameter Estimation: the estimated cardiac activation maps obtained from the *sinus rhythm* sequence were used to retrieve patient-specific conduction velocity (CV) parameters. Because the regression was performed on simulated activation maps, the resulting solution is smooth and physiologically relevant. If we consider that a normal heart QRS is less than 120ms, we make the following hypothesis : regions that are late activated during *sinus rhythm* correspond to regions of slow conduction velocity. This was motivated by the fact that cardiologists are looking at very late activated zones during sinus rhythm for locating scar from CardioInsight inverse solutions. Specifically, we threshold the estimated activation times t_a and defined 3 zones: healthy tissue ($t_a < 120ms$, $CV = 0.5m/s$), damaged tissue ($120 < t_a < 170ms$, $CV = 0.3m/s$), and scar tissue ($170 < t_a$, no reaction term and diffusion reduced by 80%). We used a single value for the healthy tissue based on a previous study where the personalised global CV were all found close to $0.5m/s$ [5].

6) Pacing Prediction and AV node Activation: We will now predict the activation maps under pacing 'as if' the patient was not implanted yet, using the measured pacing locations from CT imaging and our personalised CV parameters - before comparing with the measured pacing signals. For every patient, the measured ventricular pacing locations were segmented from the CT scanner image, however the image artifacts due to the device only allow an approximate lead location. The personalised parameters from *sinus rhythm* BSPMs were used to predict the activation maps of different pacing situations. On some patients we found on the CardioInsight inverse solution that the RV was activated without ventricular pacing, probably from the atrial pacing (100 to 200ms before) via the AV node. For these patients (#1, #2 6M, #4, #7, #9, #12, #13) we had to include in our model an AV node activation to the ventricular pacings. For that, we triggered the earliest activated zones estimated in the *sinus rhythm* result. Because no recording of atrial stimulation and AV delay were available, the triggering time was arbitrarily set to 40ms.

E. Reference Anatomy Evaluation

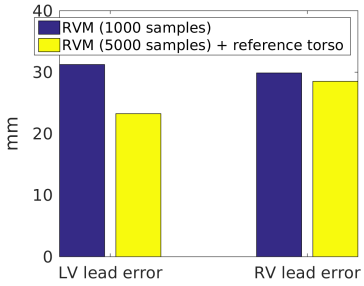

Fig. 7. Patient #3: Localization error between the previous RVR method and the presented method using the reference anatomy.

We aim at evaluating the regression using a reference anatomy by comparing it with the regression using simulations on the patient-specific torso anatomy, that already showed its efficiency [25]. The goal of this previous study was localizing two onset activation locations at the same time from a *simulateous* pacing using a 1000 patient-specific training set. We show (Figure 7) the lead localization errors of patient #3 from the previous method [25] and from the current method (using the reference anatomy, enabling also more training samples:

[2]we used a python implementation available at https://github.com/AmazaspShumik/sklearn-bayes

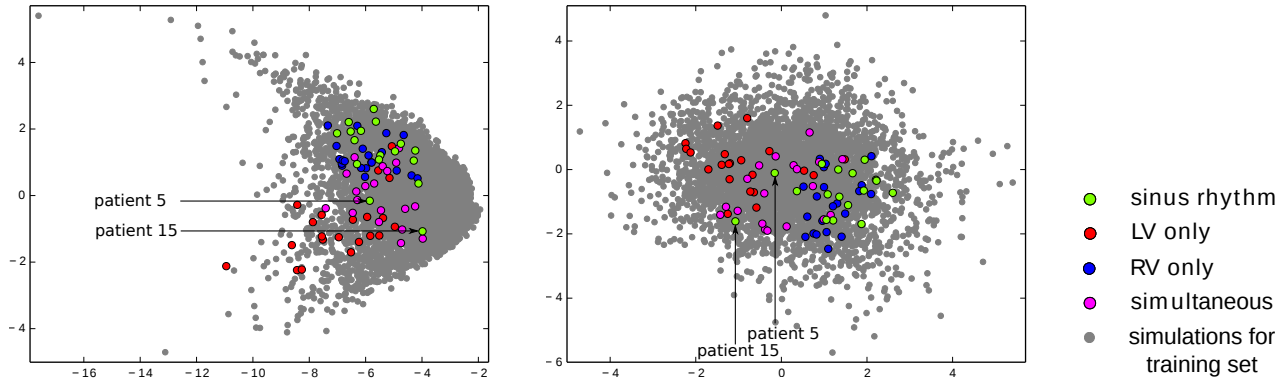

(a) projection on modes 1 and 2 (b) projection on modes 2 and 3

Fig. 8. RVR results on the reduced shape space from measured BSPM sequences of the 20 patients. Grey dots: projection of the 5000 simulated activation maps used for training.

5000). The new method shows slightly better results. The uncertainty introduced by the reference anatomy may have been alleviated by the larger database.

III. Personalisation Results and Pacing Predictions

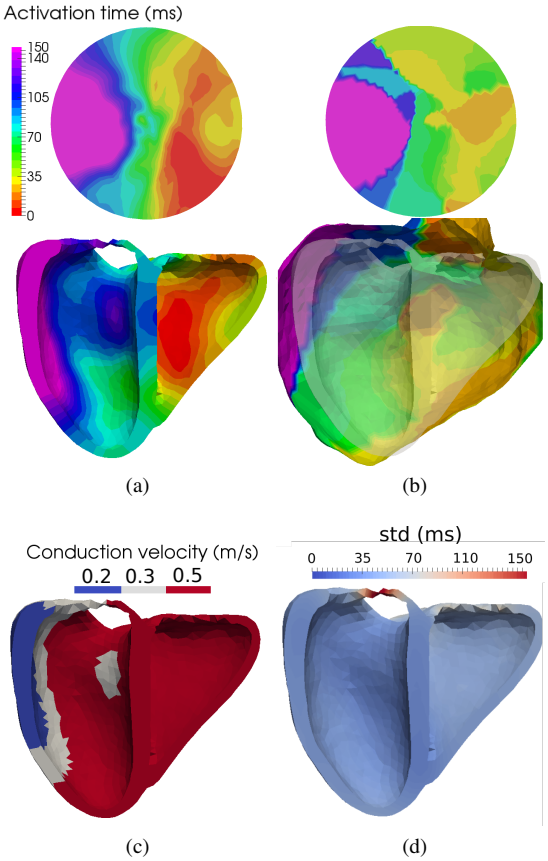

(a) (b) (c) (d)

Fig. 9. *Sinus rhythm* of patient #9 (a) estimated activation map from RVR method. *up*: flattening view of the epicardial surface. (b) CardioInsight epicardial inverse solution. (c) Personalised conduction velocity from thresholding the estimated activation map. (d) estimated standard deviation.

A. Projections on the Reduced Shape Space

In Figure 8 we showed the RVR results of each measured BSPM sequence on the reduced shape space. Because the modes of this space are related to modes of vibration, the results projected on the larger modes allow us to easily compare the BSPM sequences. Each grey point represents one simulated activation map used for training. The measured BSPMs sequences of the 20 patients are shown with colours representing the type of sequence. All the results from the measured BSPM data lie inside the training set point cloud, which is important for the RVR to perform well. We can also see that the 3 different pacing sequences are separated in clusters, with the *simultaneous* between the *RV pacing* and the *LV pacing*. The *sinus rhythm* results in green are almost all situated near the *RV pacing* cluster, which is to be expected for LBBB patients. Interestingly, we can notice that the two *sinus rhythm* exceptions that are closer to the *LV pacing* group in blue correspond to the two RBBB patients of the cohort (patients #5 and #15).

B. Estimated Sinus Rhythm Activation Maps

The RVR results of the *sinus rhythm* sequences in terms of activation map were used to estimate the local conduction velocity parameter of each patient. In Figure 9 is represented the mean solution as a transmural activation map (9a) that was compared with the CardioInsight epicardial inverse solution [31] (9b). The CardioInsight solution is interesting for comparison even if it is only an epicardial surface reconstruction. On top are flat representations of the epicardial surface [32]. The wave shape are similar, with a large late activated zone on the lateral LV wall with probable scar tissue. In Figure 9c are shown the retained zones for healthy, diseased and scar tissues from thresholding of Figure 9a. Finally, because the RVR regression provided the result as a Gaussian probability distribution in the reduced shape space, the estimated standard deviation across each mode were projected on the myocardial mesh. The zones with a high estimated standard deviation were found near the valves where the mesh is thin, and the median standard deviation was 37ms (see Figure 9d). The personalisation results of two other patients (#11 and #15)

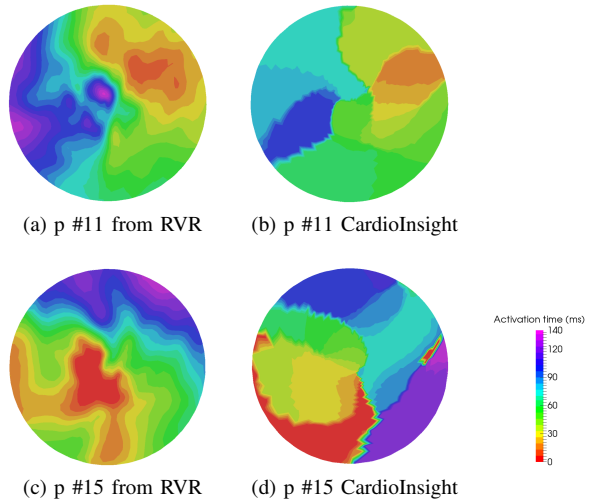

(a) p #11 from RVR (b) p #11 CardioInsight

(c) p #15 from RVR (d) p #15 CardioInsight

Fig. 10. *Sinus rhythm* of two other patients: #11 (a)(b) and #15 (c)(d). Flattening view of the epicardial surface. *Left:* Estimated activation map from RVR method. *Right:* CardioInsight epicardial inverse solution.

are compared with the CardioInsight solution in Figure 10, showing similar activation maps even for the RBBB pattern (patient #15).

C. Pacing Predictions Results

1) Predicted Activation Maps: From the CV parameters estimated using the RVR solution of the *sinus rhythm* BSPMs, we ran again our cardiac Mitchell-Schaeffer model by using the measured pacing locations provided by imaging under different conditions (*RV only*, *LV only*, *simultaneous*, *LV 40ms*, *RV 40ms*). We compared its output to the measured pacing BSPM recordings and to the CardioInsight solution. This comparison will demonstrate the proximity between a standard inverse method and a predictive method that could be performed without any pacemaker on the patient. In Figure 11 is represented the predicted *LV 40ms* activation map for patient #9 (Figure 11a), the prediction if we used a model with a homogeneous myocardial CV (Figure 11a) and the CardioInsight solution (Figure 11b). The flat representation allows for a better comparison even if the projection of the epicardium may differ between two cardiac geometries. We can see that the homogeneous CV prediction missed the scar while with the personalised CV the wave shape and timings globally correspond to CardioInsight. The area with 0.2m/s conduction velocity on the LV lateral wall indicates an infarction zone, as also visible on the CardioInsight map.

The prediction of *LV only* pacing of patient 9 is shown on Figure 12a. The predicted propagation was completely blocked by the scar zone, while an RV activation is visible on the CardioInsight solution Figure 12c. With the AV activation model (see section II-D6), the resulting activation map (Figure 12b) is closer to the CardioInsight solution. In Figure 8, we could see some *LV only* projections (red) inside the *RV only* point cloud: they correspond to patients 1, 9 and 12 all showing a separate RV activation and also an important LV late activated near the LV pacing lead.

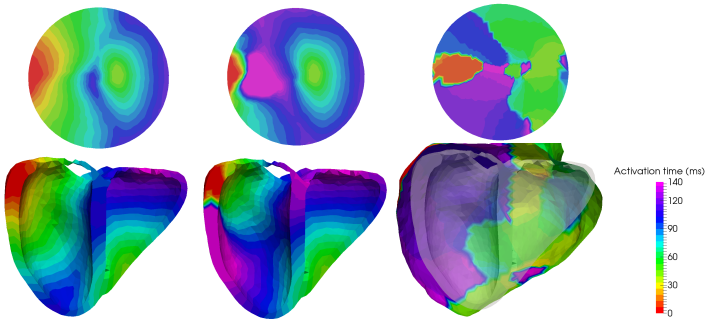

(a) homogeneous CV (b) estimated CV (c) CardioInsight

Fig. 11. *LV 40ms* pacing prediction of patient #9, long-axis and flattening epicardial representations of the activation maps (a) pacing prediction using homogeneous conduction velocity ;(b) using the personalised parameters from *sinus rhythm*; (c) CardioInsight inverse solution of the actual pacing.

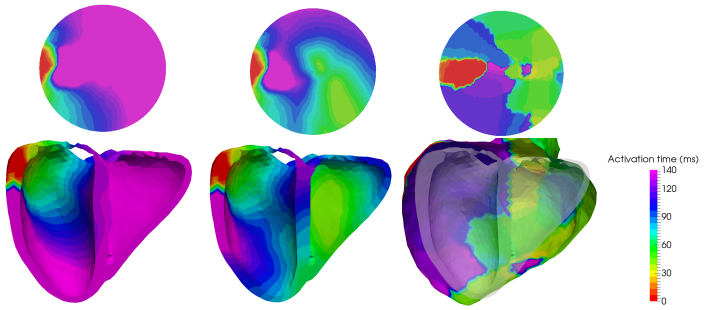

(a) estimated CV (b) AV node active (c) CardioInsight

Fig. 12. *LV only* pacing prediction of patient #9, long-axis and flattening epicardial representations. (a) using the personalised parameters from *sinus rhythm*; (b) adding the modelled activation of the AV node after 40ms; (c) CardioInsight inverse solution from actual recordings of the pacing.

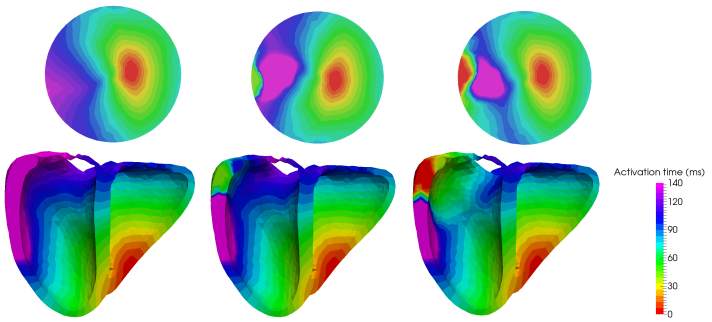

(a) *RV only* (b) *RV 40ms* (c) *simultaneous*

Fig. 13. Other pacing predictions of patient #9, long-axis and flattening epicardial representations. (a) *RV only* (b) *RV 40ms*; (c) *simultaneous*.

As a quantitative comparison, Figure 14 shows the activation times differences on the flat epicardium, between our predictions and the CardioInsight inverse solutions on 20 patients. The total median difference is 23.8ms. It indicates some similar activation patterns even if few points have an important difference (higher than 50ms). A perfect match is difficult because of the epicardial projections difference, the piece-wise constant CardioInsight solution and the approximation in the pacing electrodes locations. We can notice that the *LV only* seems to be the more difficult to predict.

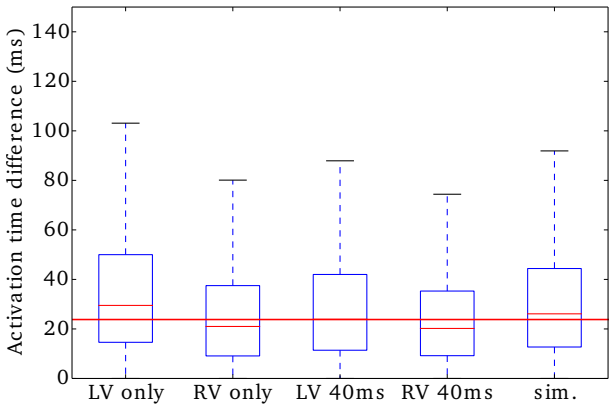

Fig. 14. Prediction of pacing activation maps (20 patients): activation times differences on the flattened epicardial points, between our prediction and the CardioInsight inverse solution. Median difference (red line): 23.8ms.

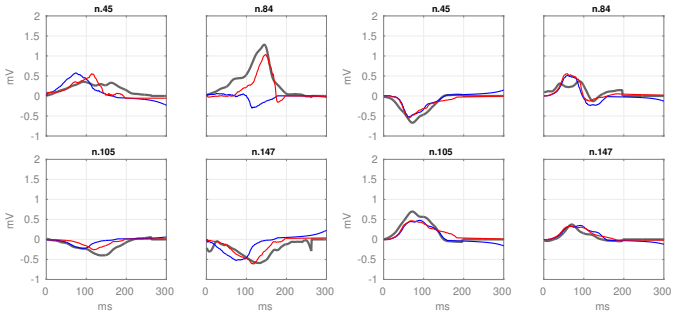

(a) *LV only* prediction (b) *RV only* prediction

Fig. 15. Pacing predictions of patient #3, example of BSPM signals. *Gray:* Ground truth signal; *blue:* pacing prediction with a homogeneous myocardial CV; *red:* pacing prediction with a personalised CV from *sinus rhythm*.

2) BSPM predictions: We also predicted the corresponding pacing BSPM signals and compared them with the measured signals. Some signal examples of pacing predictions from patient #3 (Figure 15) showed a clear improvement when using the personalised CV for the *LV only*, while the homogeneous CV shows already a good agreement for the *RV only*. In Figure 16 we can see the averaged correlation coefficients ($\overline{CC}$) between measured and predicted BSPM signals. Because the cardiac geometry was generic and the pacing locations not accurate, we cannot expect a perfect match between BSPMs. However, we can see that the mean $\overline{CC}$ of every pacing type increases when the local CV was personalised from *sinus rhythm*. In particular, the effects on the *LV only* prediction are highest because the LV damaged tissues can have higher impacts on the wave propagation. We can still see some outliers having low $\overline{CC}$ values. The lowest one (from patient #16) corresponds to the *LV only* outlier (red) in the projected modes of Figure 8a, in a zone where the training simulations are sparse. It might indicate that our training set did not cover properly this region of the parameter space.

IV. Discussion

A. Reference Anatomy

The interpatient study could be a useful tool for different applications, as it also allows some comparison between

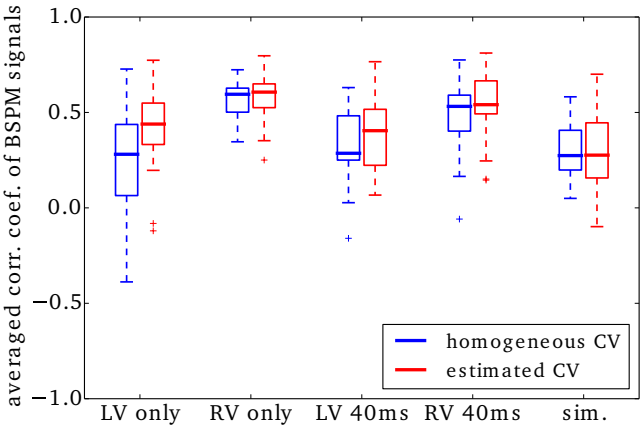

Fig. 16. Prediction of pacing activation maps (20 patients): averaged correlation coefficient ($\overline{CC}$) between measured and predicted BSPM signals. In blue, the prediction was performed with a homogeneous myocardial conduction velocity. In red is the result with the CV personalised from *sinus rhythm* (and with the AV activation in patients 1, 2 6M, 4, 7, 9, 12, 13).

patients. However, it is not universal because our template has a large number of electrodes on both sides of the torso. A new dataset composed of only frontal electrodes would not be correctly projected on the back. The use of a simpler reference with fewer electrodes could be a more general alternative.

We used a reference cardiac geometry, where the size of the heart was fixed. We evaluated the impact of the cardiac scaling on the simulated resulting BSPM signals. Two cardiac scalings of ratios 0.8 and 1.7 to the original size were tested (corresponding to extreme sizes). The center of mass of the myocardium was taken as origin. The resulting normalized BSPM signals showed a relative mean signal difference of 0.1% for the 0.8 scaling ratio and 0.2% for the 1.7 scaling ratio. We can deduce that the size of the heart can be neglected if an appropriate origin is chosen. We did not quantify the error caused by local cardiac shape differences, as the precise patient-specific cardiac anatomy was not available (due to imaging artifacts caused by the pacemaker).

In our setting, the heart location and orientation was segmented from CT scan images. We think that this ionising and computational procedure could be replaced by an estimation of the position and orientation parameters, either by statistical prediction from easy patient characteristics [33] or by simultaneous EP inverse optimization [34], [35].

B. Estimating conduction velocity from activation times

In this work we personalised the local conduction velocity parameter by assigning low values on late activated zones. The direct estimation of local velocity from an activation map raises many challenges (because of the mesh, the anisotropy, the direction of the wave), even though some recent studies are proposing new approaches [36], [37]. Their use could improve our estimation and thus the predictions, as our translation from activation times into conduction velocity has to be handled with care and might be wrong in some cases.

C. Estimating the uncertainty

The RVR standard deviation is a by-product of the regression and can be a way to interpret the regression uncertainty. However, a proper posterior distribution would be useful for a better accuracy and for identifying the stability of the solution. The use of surrogate modelling into a Metropolis Hasting sampling was recently proposed [38]. We could then also integrate the other sources of uncertainty as the mean torso sensor distance to the template.

D. AV node Activation

We have seen that some patients were activated also from an atrial pacing via the AV node. We have modelled it with an arbitrary time delay, but we think it would be possible to integrate it with more complete data (if the atrial stimulation was recorded). Moreover, the integration of the atria in the ventricular model (for example as a thin layer [39]) and a study of the whole heart beat ECG could be beneficial for a precise and global personalisation.

V. Conclusion

We have developed a methodology for solving the ECG inverse problem and estimating local cardiac conductivity parameters using a physiological model-based regression on a reference anatomy. The data matching to the template anatomy allowed us to use a large offline simulated database of EP forward models for the regression of the BSPM signals from 20 patients with a CRT indication. We used a sparse Bayesian kernel-based regression for the estimation of cardiac activation maps with the use of specific BSPM descriptors and a reduced space for the myocardial geometry. From the CV parameters estimated with the *sinus rhythm* BSPM sequence, we predicted the responses to different pacing conditions. We compared them with the measured pacing BSPMs and with a commercially available epicardial inverse solution (median activation time difference: 24ms). While a validation with intracardiac recordings is still necessary, we believe that the small patient-specific computational time (less than 2 minutes) can be crucial for a clinical use. We predicted the patient-specific EP response to different pacing configurations, which are useful for the clinician in order to identify CRT responders. It is a first step to an identification of CRT responders from modelling, where we would also need some mechanical output predictions (such as the ejection fraction).

Acknowledgment

The research leading to these results has received European funding from the Seventh Framework Programme (FP7/2007-2013) under grant agreement VP2HF n°611823 and ERC starting grant ECSTATIC (715093).

References

[1] O. Dössel, "Inverse problem of electro-and magnetocardiography: Review and recent progress," *International Journal of Bioelectromagnetism*, vol. 2, no. 2, 2000.

[2] M. G. S. J. Sutton *et al.*, "Effect of cardiac resynchronization therapy on left ventricular size and function in chronic heart failure," *Circulation*, vol. 107, no. 15, pp. 1985–1990, 2003.

[3] M. Sermesant *et al.*, "Patient-specific electromechanical models of the heart for the prediction of pacing acute effects in crt: A preliminary clinical validation," *Medical image analysis*, vol. 16, no. 1, pp. 201–215, 2012.

[4] G. Li and B. He, "Localization of the site of origin of cardiac activation by means of a heart-model-based electrocardiographic imaging approach," *IEEE Transactions on biomedical engineering*, vol. 48, no. 6, pp. 660–669, 2001.

[5] S. Giffard-Roisin *et al.*, "Noninvasive personalization of a cardiac electrophysiology model from body surface potential mapping," *IEEE Transactions on Biomedical Engineering*, vol. 64, no. 9, pp. 2206–2218, 2017.

[6] J. Dhamala *et al.*, "Spatially-adaptive multi-scale optimization for local parameter estimation in cardiac electrophysiology," *IEEE Transactions on Medical Imaging*, 2017.

[7] A. J. Pullan, "The inverse problem of electrocardiography," in *Comprehensive Electrocardiology*. Springer London, 2010, pp. 299–344.

[8] C. Han *et al.*, "Imaging cardiac activation sequence during ventricular tachycardia in a canine model of nonischemic heart failure," *American Journal of Physiology-Heart and Circulatory Physiology*, vol. 308, no. 2, pp. H108–H114, 2014.

[9] L. Yu, Z. Zhou, and B. He, "Temporal sparse promoting three dimensional imaging of cardiac activation," *IEEE transactions on medical imaging*, vol. 34, no. 11, pp. 2309–2319, 2015.

[10] Z. Zhou *et al.*, "Noninvasive imaging of high-frequency drivers and reconstruction of global dominant frequency maps in patients with paroxysmal and persistent atrial fibrillation," *IEEE Transactions on Biomedical Engineering*, vol. 63, no. 6, pp. 1333–1340, 2016.

[11] L. Yu *et al.*, "Three-dimensional noninvasive imaging of ventricular arrhythmias in patients with premature ventricular contractions," *IEEE Transactions on Biomedical Engineering*, 2017.

[12] A. Rahimi *et al.*, "Examining the impact of prior models in transmural electrophysiological imaging: A hierarchical multiple-model bayesian approach," *IEEE Transactions on Medical Imaging*, vol. 35, no. 1, pp. 229–243, 2016.

[13] L. Wang *et al.*, "Noninvasive computational imaging of cardiac electrophysiology for 3-d infarct," *IEEE Transactions on biomedical engineering*, vol. 58, no. 4, pp. 1033–1043, 2011.

[14] C. Liu *et al.*, "Estimation of global ventricular activation sequences by noninvasive three-dimensional electrical imaging: Validation studies in a swine model during pacing," *Journal of cardiovascular electrophysiology*, vol. 19, no. 5, pp. 535–540, 2008.

[15] T. Yang *et al.*, "Localization of origins of premature ventricular contraction by means of convolutional neural network from 12-lead ecg," *IEEE Transactions on Biomedical Engineering*, 2017.

[16] R. Hoekema *et al.*, "Interindividual variability of multilead electrocardiographic recordings: influence of heart position," *Journal of electrocardiology*, vol. 32, no. 2, pp. 137–148, 1999.

[17] D. J. Swenson *et al.*, "Cardiac position sensitivity study in the electrocardiographic forward problem using stochastic collocation and boundary element methods," *Annals of biomedical engineering*, vol. 39, no. 12, p. 2900, 2011.

[18] G. Huiskamp and A. van Oosterom, "Tailored versus realistic geometry in the inverse problem of electrocardiography," *IEEE Transactions on Biomedical Engineering*, vol. 36, no. 8, pp. 827–835, 1989.

[19] J. Lenkova, J. Svehlikova, and M. Tysler, "Individualized model of torso surface for the inverse problem of electrocardiology," *Journal of electrocardiology*, vol. 45, no. 3, pp. 231–236, 2012.

[20] L. Wang *et al.*, "How much geometrical detail do we need in cardiac electrophysiological imaging? A generic heart-torso representation for fast subject-specific customization," in *STACOM Workshop, held in Conjunction with MICCAI Conference*, 2010, pp. 232–241.

[21] A. Rahimi and L. Wang, "Sensitivity of noninvasive cardiac electrophysiological imaging to variations in personalized anatomical modeling," *IEEE Transactions on Biomedical Engineering*, vol. 62, no. 6, pp. 1563–1575, 2015.

[22] S. Chen *et al.*, "Disentangling inter-subject variations: Automatic localization of ventricular tachycardia origin from 12-lead electrocardiograms," in *ISBI Conference*, 2017, pp. 616–619.

[23] J. Malmivuo and R. Plonsey, *Bioelectromagnetism: principles and applications of bioelectric and biomagnetic fields*. Oxford university press, 1995.

[24] C. C. Mitchell and D. G. Schaeffer, "A two-current model for the dynamics of cardiac membrane," *Bulletin of mathematical biology*, vol. 65, no. 5, pp. 767–793, 2003.

[25] S. Giffard-Roisin *et al.*, "Sparse bayesian non-linear regression for multiple onsets estimation in non-invasive cardiac electrophysiology," in *FIMH Conference*. Springer, 2017, pp. 230–238.
[26] N. Duchateau *et al.*, "Infarct localization from myocardial deformation: prediction and uncertainty quantification by regression from a low-dimensional space," *IEEE Transactions on Medical Imaging*, vol. 35, no. 10, pp. 2340–2352, 2016.
[27] M. Reuter, F.-E. Wolter, and N. Peinecke, "Laplace-spectra as fingerprints for shape matching," in *ACM symposium on Solid and physical modeling*. ACM, 2005, pp. 101–106.
[28] S. Umeyama, "An eigendecomposition approach to weighted graph matching problems," *IEEE Transactions on pattern analysis and machine intelligence*, vol. 10, no. 5, pp. 695–703, 1988.
[29] M. E. Tipping, A. C. Faul *et al.*, "Fast marginal likelihood maximisation for sparse bayesian models." in *AISTATS*, 2003.
[30] C. M. Bishop and M. E. Tipping, "Variational relevance vector machines," in *Proceedings of the conference on Uncertainty in artificial intelligence*. Morgan Kaufmann Publishers Inc., 2000, pp. 46–53.
[31] C. Ramanathan *et al.*, "Noninvasive electrocardiographic imaging (ecgi): application of the generalized minimal residual (gmres) method," *Annals of Biomedical Engineering*, vol. 31, no. 8, pp. 981–994, 2003.
[32] D. Soto-Iglesias *et al.*, "Integration of electro-anatomical and imaging data of the left ventricle: an evaluation framework," *Medical image analysis*, vol. 32, pp. 131–144, 2016.
[33] F. Odille *et al.*, "Statistical variations of heart orientation in healthy adults," in *Computing in Cardiology Conference, Rennes*. IEEE, 2017.
[34] M. Rodrigo *et al.*, "Solving inaccuracies in the heart position and orientation for inverse solution by using electric information," in *Computing in Cardiology Conference, Rennes*. IEEE, 2017.
[35] J. Coll-Font, "Model based approaches to incorporate recordings of multiple heartbeats into the inverse problem of electrocardiography," Ph.D. dissertation, Northeastern University, 2016.
[36] A. N. Doshi *et al.*, "Feasibility of a semi-automated method for cardiac conduction velocity analysis of high-resolution activation maps," *Computers in biology and medicine*, vol. 65, pp. 177–183, 2015.
[37] J. Duchateau, M. Potse, and R. Dubois, "Spatially coherent activation maps for electrocardiographic imaging," *IEEE Transactions on Biomedical Engineering*, vol. 64, no. 5, pp. 1149–1156, 2017.
[38] J. Dhamala *et al.*, "Quantifying the uncertainty in model parameters using gaussian process-based markov chain monte carlo: An application to cardiac electrophysiological models," in *IPMI Conference*. Springer, 2017, pp. 223–235.
[39] E. Schenone, "Reduced order models, forward and inverse problems in cardiac electrophysiology," Ph.D. dissertation, Université Pierre et Marie Curie-Paris VI, 2014.